ADVANCED THERAPEUTICS
www.advtherap.com

Project IDentif.AI: Harnessing Artificial Intelligence to Rapidly Optimize Combination Therapy Development for Infectious Disease Intervention

Aynur Abdulla, Boqian Wang, Feng Qian, Theodore Kee, Agata Blasiak, Yoong Hun Ong, Lissa Hooi, Falgunee Parekh, Rafael Soriano, Gene G. Olinger, Jussi Keppo, Chris L. Hardesty, Edward K. Chow, Dean Ho, and Xianting Ding**

In 2019/2020, the emergence of coronavirus disease 2019 (COVID-19) resulted in rapid increases in infection rates as well as patient mortality. Treatment options addressing COVID-19 included drug repurposing, investigational therapies such as remdesivir, and vaccine development. Combination therapy based on drug repurposing is among the most widely pursued of these efforts. Multi-drug regimens are traditionally designed by selecting drugs based on their mechanism of action. This is followed by dose-finding to achieve drug synergy. This approach is widely-used for drug development and repurposing. Realizing synergistic combinations, however, is a substantially different outcome compared to globally optimizing combination therapy, which realizes the best possible treatment outcome by a set of candidate therapies and doses toward a disease indication. To address this challenge, the results of Project IDentif.AI (Identifying Infectious Disease Combination Therapy with Artificial Intelligence) are reported. An AI-based platform is used to interrogate a massive 12 drug/dose parameter space, rapidly identifying actionable combination therapies that optimally inhibit A549 lung cell infection by vesicular stomatitis virus within three days of project start. Importantly, a sevenfold difference in efficacy is observed between the top-ranked combination being optimally and sub-optimally dosed, demonstrating the critical importance of ideal drug and dose identification. This platform is disease indication and disease mechanism-agnostic, and potentially applicable to the systematic N-of-1 and population-wide design of highly efficacious and tolerable clinical regimens. This work also discusses key factors ranging from healthcare economics to global health policy that may serve to drive the broader deployment of this platform to address COVID-19 and future pandemics.

A. Abdulla, B. Wang, Prof. X. Ding
Institute for Personalized Medicine
School of Biomedical Engineering
Shanghai Jiao Tong University
Shanghai 200030, China
E-mail: dingxianting@sjtu.edu.cn
Prof. F. Qian
Ministry of Education Key Laboratory of Contemporary Anthropology
Human Phenome Institute
School of Life Sciences
Fudan University
Shanghai 200438, China

The ORCID identification number(s) for the author(s) of this article can be found under https://doi.org/10.1002/adtp.202000034

DOI: 10.1002/adtp.202000034

T. Kee, Dr. A. Blasiak, Y. H. Ong, Prof. E. K. Chow, Prof. D. Ho
The N.1 Institute for Health (N.1)
National University of Singapore
Singapore 117456, Singapore
E-mail: biedh@nus.edu.sg
T. Kee, Dr. A. Blasiak, Prof. D. Ho
The Institute for Digital Medicine (WisDM)
Yong Loo Lin School of Medicine
National University of Singapore
Singapore 11756, Singapore
T. Kee, Dr. A. Blasiak, Prof. D. Ho
Department of Biomedical Engineering
NUS Engineering
National University of Singapore
Singapore 117583, Singapore
L. Hooi, Prof. E. K. Chow
Cancer Science Institute of Singapore
National University of Singapore
Singapore 117599, Singapore
Dr. F. Parekh, R. Soriano
EpiPointe
LLC
Cary, NC 27518, USA

1. Introduction

The discovery of COVID-19 has led to global panic and substantial challenges in rapidly and systematically identifying suitable interventions for this unpredictable disease.[1] Similar challenges have been associated with severe acute respiratory syndrome (SARS),[2] H1N1,[3] H7N9,[4] Middle East Respiratory Syndrome (MERS),[5] and Ebola Virus Disease (EVD),[6] among others. When addressing infectious diseases that are not well understood, and capable of exhibiting aggressive clinical courses with subsequent patient mortality, rapid intervention that is optimally suited to target the pathogen is critical. Due to the unpredictability and severity of these pathogens, combination therapy based on drug repurposing is often indicated due to the urgency of intervention and the requirement of previously established drug safety in humans. Unfortunately, these drug combinations are often designed using trial-and-error strategies. Specifically, drugs are selected based on their targets or mechanism of action, and they are administered using clinical standard dosing guidelines. Dose adjustments are made when toxicity is observed. Unfortunately, these approaches likely preclude optimal treatment outcomes.

Previously, a broad spectrum of methodologies have been used as part of multiple important studies to develop combination therapies to address multiple disease indications.[7] Substantial efforts have also been directed toward new drug development. When confronted with a novel pathogen strain with high virulence, a potential capacity for rapid and continuous mutation, and poor patient outcomes, the global community often requires rapidly actionable responses due to patient mortality that may quickly follow initial diagnosis. To address the COVID-19 crisis, a substantial number of clinical trials have been initiated.[8] Treatment options explored to address COVID-19 have included repurposed human immunodeficiency virus (HIV) and influenza-related monotherapies and drug cocktails, trials of investigational therapies such as remdesivir (Gilead Sciences), and has sparked a worldwide effort to develop a vaccine. Among large sets of candidate therapies for drug repurposing in combination therapy, standard approaches involve drug selection based on mechanism of action. Drug dosing is subsequently determined by established clinical guidelines. Traditional design approaches are based on trial-and-error, and barriers include sub-optimal efficacy and dose-limiting toxicities. In sum, the lack of a systematic way to interrogate the massive drug-dose parameter space created by these pools of candidate therapies preclude the ability to optimize treatment outcomes.

To address this challenge, this work reports the outcomes of Project IDentif.AI, which harnesses an AI-based platform to interrogate drug and dose parameter spaces that are insurmountably large for brute-force testing of all possible combinations. Project IDentif.AI sought to determine the duration of time required to simultaneously identify the best drugs and doses from a pool of 12 candidate therapies that optimally inhibited the infection of the A549 lung cell line by VSV (efficacy) while maintaining A549 (efficacy). These therapies included amantadine HCl, dexamethasone, azithromycin, chloroquine diphosphate, naproxen sodium, fluoxetine HCl, loratadine, omeprazole sodium, ritonavir, lopinavir, doxycycline and ribavirin. The 12 candidate therapies were selected based on multiple factors that may be considered during pandemics, including prior studies examining their role as repurposed monotherapies in addressing a diverse range of viral pathogens, global adoption and availability of the therapies, as well as tolerability by broad classes of patients, among others. Specifically, Amantadine HCl is an organic compound that was developed to address influenza infections.[9] It has been repurposed for treatment of motor impairment in Parkinson's disease,[10] and explored for improvement of fatigue in patients with multiple sclerosis.[11] Dexamethasone is a potent anti-inflammatory and immunosuppressant glucocorticoid. It is used in therapies against a wide range of indications, including oncology and bacterial infections.[12] It has been successfully used to treat dengue-related hemophagocytic syndrome.[13] Azithromycin is an antibiotic given to patients with bacterial infections of lower respiratory tract,[14] including community-acquired pneumonia.[15] It has been explored as a novel antimalarial agent.[16] Chloroquine disphosphate is the most widely used drug against malaria. In recent years it has been found to target other infectious diseases, including HIV and fungal infections.[17] Naproxen sodium is an established nonselective, nonsteroidal anti-inflammatory drug (NSAID) commonly used for treating mild and moderate pain and inflammation.[18] Recently, It has been shown to act against influenza A and B viruses.[19] Fluoxetine HCL, widely known as Prozac, is an antidepressant used to treat a range of depressive disorders.[20] Its antiviral properties have been explored for treating coxsackievirus.[21] Loratadine is a second-generation nonsedating antihistamine used for allergies.[22] Recent clinical trials have evaluated its use as abortive therapy in pegfilgrastim-associated bone pain.[23] Omeprazole sodium is a proton pump inhibitor (PPI) used to treat gastrointestinal reflux disease and in *Helicobacter pylori* eradication therapy for gastritis and peptic ulcers.[24] Omeprazole and other PPIs have recently been investigated for and demonstrated antitumor activity and anti-inflammatory effects.[25] Ritonavir and lopinavir are antiretroviral medications commonly used in combination treatment for patients infected with (HIV), with ritonavir used as a booster with other protease inhibitors like lopinavir.[26] Lopinavir and ritonavir combination has demonstrated in vitro antiviral

Dr. G. G. Olinger
Global Health Surveillance and Diagnostic Division
MRIGlobal
Gaithersburg, MD 20878, USA
Dr. G. G. Olinger
Boston University School of Medicine
Division of Infectious Diseases
Boston, MA 02118, USA
Prof. J. Keppo
NUS Business School and Institute of Operations Research and Analytics
National University of Singapore
Singapore 119245, Singapore
C. L. Hardesty
KPMG Global Health and Life Sciences Centre of Excellence
Singapore 048581, Singapore
Prof. E. K. Chow, Prof. D. Ho
Department of Pharmacology
Yong Loo Lin School of Medicine
National University of Singapore
Singapore 117600, Singapore

activity against SARS and favorable clinical response in patients with SARS.[27] Ritonavir has also been explored and shown to be highly effective as a booster in fixed-dose combinations for patients with Hepatitis C.[27] Doxycycline is a tetracycline antibiotic with a broad antimicrobial spectrum of activity.[28] In recent clinical trials, doxycycline has been shown to treat nasal polyps and rosacea, as an anti-inflammatory.[29] Ribavirin is an antiviral medication often administered in combination with interferon-based therapies for patients with chronic Hepatitis C.[30] Additionally, Ribavirin has been shown to be an effective treatment for respiratory syncytial virus and hemorrhagic fevers.[31]

Within 3 days, our studies successfully identified and repeatedly validated multiple drug combinations that simultaneously reduced VSV infection to 1.5% with no apparent adverse impact on A549 viability. In addition, this platform identified multiple highly efficacious and tolerable regimens, presenting the potential of multiple options for treatment. This study demonstrated that Project IDentif.AI can potentially be used for patient-specific or population-wide development of actionable combination therapy. It's implementation also does not require complex disease mechanism or drug target information for implementation. This may enable its immediate application toward dynamically-optimized drug repurposing and novel combination therapy development against high priority pathogens such as COVID-19 and others.

In addition to reporting rapid experimentally identified and validated combination therapies against VSV infection of A549, this work also discusses key further studies needed, and provides global health and healthcare economics policy perspectives that may provide a roadmap toward the broader clinical deployment of Project IDentif.AI. Collectively, these analyses demonstrate that technology and innovative policy considerations are needed to drive advances in clinical practice in addressing pre-pandemic and pandemic challenges.

2. Results

2.1. Optimization of Cell Density, VSV Incubation Time and Multiplicity of Infection (MOI)

The VSV model used for this study was encoded with green fluorescent protein (GFP) to monitor cell infection, with GFP intensity corresponding to viral infection efficiency. The GFP intensity of VSV-infected cells under different MOI parameters (0.125, 0.25, 0.5, 1) were assessed. Cell densities for each well of 96 well plate varied between 4000 (4k), 8000 (8k) and 12 000 (12k) per well. Infection was allowed for 24 and 30 h (**Figure 1**A,B). As indicated in the figure and microscopic images, MOI as low as 0.125 was sufficient to mediate nearly 100% cell infection after 24 h for 12k per well initial cell density. We therefore utilized 12k per well as the initial cell density throughout the study. We then further reduced the MOI and incubation time. Microscope images of bright field and fluorescence are merged for visualization under different MOI parameters (0.001, 0.01, 0.1) after VSV infection occurred for 12 h (Figure 1C) and 24 h (Figure 1D). Of note, as indicated in the Figure 1C and ImageJ cell counting results, only $9.56 \pm 2.55\%$ ($n = 3$) cells were infected under MOI = 0.001 during 12 h. A MOI = 0.01 infected a majority of the cells after a 12 h incubation and the overall GFP intensity continued to increase at the 24 h checkpoint, indicating that the virus continued its reproduction inside the cells during this period of time.

2.2. Single Drug Dose Response Curves for Cell Viability and Viral Infection

In order to assess single drug toxicity and antiviral efficacy, single drug-dose response curves were acquired. Cell viability was assessed at 24 h and VSV infection was recorded at 12 and 24 h at an initial cell density of 12k per well. The MOI was maintained at 0.01. The VSV and drugs were simultaneously added to the host cells for co-incubation. Dose response curves for Amantadine HCl (AMT); Dexamethasone (DEX); Azithromycin (AZT); Chloroquine Diphosphate (CLR); NPX, Naproxen Sodium (NPX); Fluoxetine HCl (FLX); LRT, Loratadine (LRT); Omeprazole Sodium (OMP); Ritonavir (RTN); Lopinavir (LPN); Doxycycline (DOX); Ribavirin (RBV) (**Figure 2**). NPX and RBV were tested at concentrations of 0.5, 5, 50, and 500×10^{-6} M while all the remaining drugs were tested at concentrations of 0.1, 1, 10, and 100×10^{-6} M (Table S1, Supporting Information). As monotherapies, none of the drugs were able to mediate viral infection levels below 5%. With the exception of AZT, FLX, LRT, LPN and DOX, which mediated observable toxicity at high concentrations, the candidate monotherapies and their studied concentration ranges appeared tolerable (over 75% cell viability). Of note, the final DMSO concentration for all the tests did not exceed 0.3% to ensure the cell viability can be attributed to drug treatments.

2.3. Artificial Intelligence-Based Optimization of Combination Therapy from a 12-Drug Pool

The core aim of Project IDentif.AI was to simultaneously identify the combinatorial drugs and doses that optimally inhibited VSV infection of A549 while maximizing A549 viability. In lieu of using prior information pertaining to the synergistic affects among the 12 candidate drugs to identify suitable drug combinations, Project IDentif.AI harnessed a quadratic relationship between drug/dose inputs and efficacy/safety outputs to effectively identify the drug-dose parameter space from which the optimal drug combinations could be pinpointed, and drug synergy was identified after the optimization process was completed. Therefore, this process was agnostic to disease mechanism, as well as drug target information. The viral infection outcomes from each drug treatment were recorded at 12 and 24 h. For the purposes of evaluating the speed of optimization that would also yield experimentally validated VSV inhibition from a 12-drug set, a minimum threshold of 72 drug combinations with a broad range of corresponding dose levels were initially assessed (MOI = 0.1, Table S2, Supporting Information). Viral infection and drug treatment was simultaneously applied to host cells. The efficacy and corresponding accumulative equivalent dose of the 72 drug combinations revealed a broad spectrum of VSV infection rates (**Figure 3**A). The capacity for infection inhibition of each drug, as well as the quantitative interaction with the other drugs in the 12-drug pool were evaluated with the STRICT algorithm at 12 h (Figure 3B) and 24 h (Figure 3C). Of note, the key therapies that were shown to contribute toward viral inhibition when

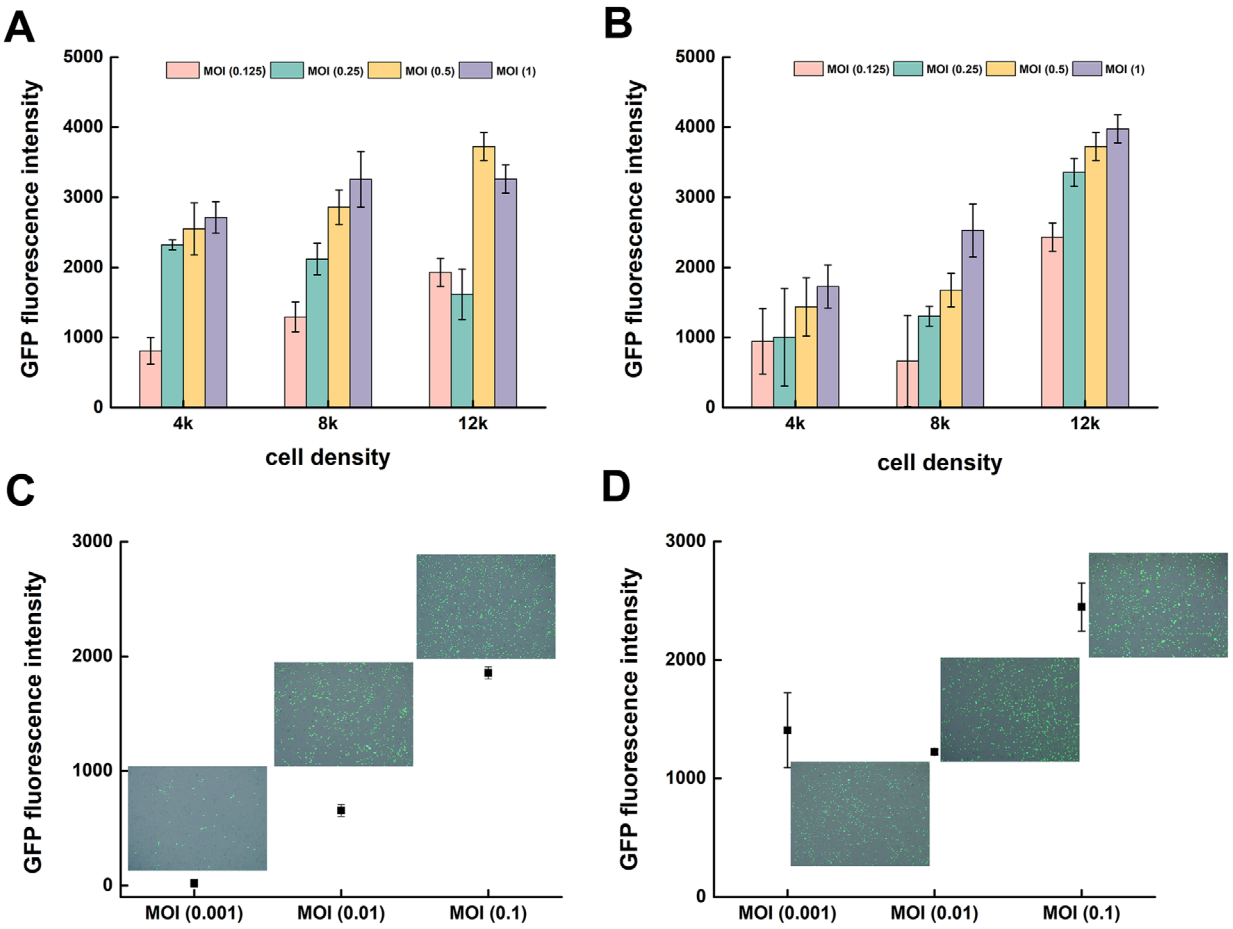

Figure 1. Optimization of cell density, VSV incubation time and multiplicity of infection (MOI). A) GFP intensity of VSV infected cells under different MOI (0.125, 0.25, 0.5, 1) for 24 h. Cell densities varied between 4k, 8k, and 12k per well of 96 well plate. Error bars show standard deviations ($n = 3$). B) GFP intensity of VSV infected cells under different MOI (0.125, 0.25, 0.5, 1) for 30 h. Cell densities varied between 4k, 8k, and 12k per well of 96 well plate. Error bars show standard deviations ($n = 3$). C) Microscope images of bright field and fluorescence are merged for visualization under different MOI (0.001, 0.01, and 0.1) after VSV infection occurred for 12 h for cells plated at 12k per well. Error bars show standard deviations ($n = 3$). D) Microscope images of bright field and fluorescence are merged for visualization under different MOI (0.001, 0.01, and 0.1) after VSV infection occurred for 24 h for cells plated at 12k per well. Error bars show standard deviations ($n = 3$).

delivered in combination with other candidates, and merit further optimization included amantadine HCl, azithromycin, chloroquine diphosphate, omeprazole sodium, and ribavirin.

Of note, some of the candidate drugs performed well as monotherapies. However, this is a common observation in in vitro platforms, and there is a subsequent need to ultimately incorporate these drugs into clinically actionable combination therapy regimens in order to optimize their use against a pathogen in question, despite their promising single drug activity. Importantly, sufficient testing of the drug-dose parameter space may also reveal that drugs with promising monotherapy activity do not belong in the optimal combination therapy regimens, which has been commonly observed using our platform.[32]

2.3.1. Systematic Validation of Optimized Combination Regimens from a 5-Drug Pool

To validate the combination regimens of the 5 candidate drugs that were advanced for further consideration, we conducted a subsequent round of experiments with 30 combinations consisting of these 5 drugs (MOI = 0.1, Table S3, Supporting Information). Viral infection and drug treatment was simultaneously applied to host cells. The viral infection from each drug treatment was recorded at 12 h (**Figure 4**A). A parabolic polynomial model was built with stepwise regression following the combinatorial optimization studies. When assessing the drug interaction coefficients as well as the parabolic response surfaces, broad synergy was subsequently observed (Figure 4B–D; Equation S1, Supporting Information). The optimal combination (Optimal Combo 1) mediated a 1.5% VSV infection rate compared to no drug treatment and was comprised of Amantadine HCl (5×10^{-6} M), Azithromycin (5×10^{-6} M), Chloroquine Diphosphate (0.5×10^{-6} M), and Ribavirin (2.5×10^{-6} M). Optimal Combo 2 mediated an infection rate of 1.6% compared to no drug treatment and was comprised of Amantadine HCl (5×10^{-6} M), Azithromycin (5×10^{-6} M), Chloroquine Diphosphate (0.5×10^{-6} M), and Omeprazole Sodium (0.5×10^{-6} M) (**Table 1**). Of note, both of these combinations were based on individual drug doses that were lower than the high doses needed to

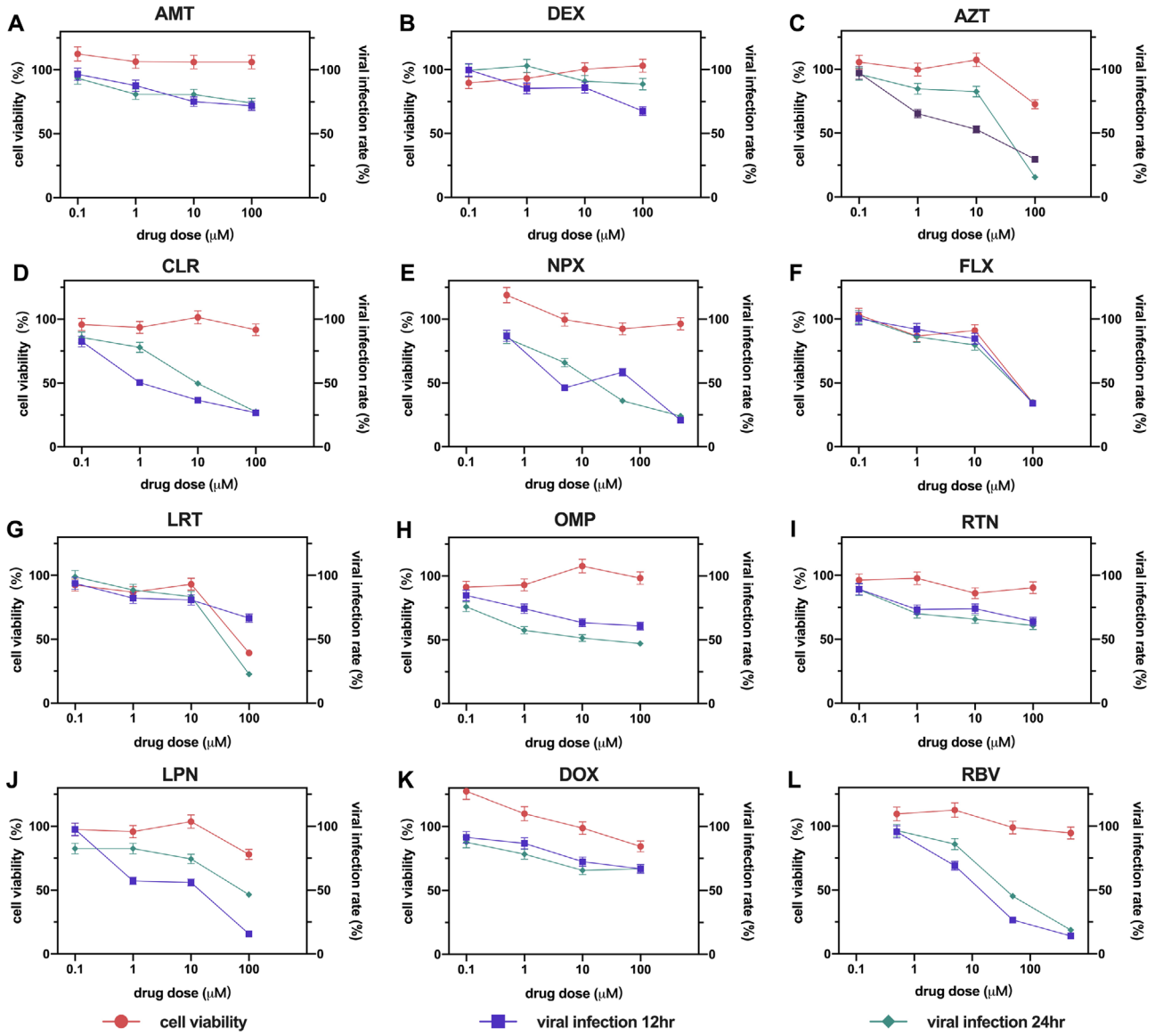

Figure 2. A–L) Single drug dose response curves for cell viability and viral infection. Cell viability is accessed at 24 h and normalized to the untreated control without being treated with drugs or virus. VSV infection is recorded at 12 and 24 h and normalized to the untreated control which only be treated with virus. Initial cell density is 12k per well in 96 well plate. MOI is 0.01. VSV and drugs are simultaneously added to host cells for co-incubation. Dose response curves for drugs. Abbreviations: AMT, Amantadine HCl; DEX, Dexamethasone; AZT, Azithromycin; CLR, Chloroquine Diphosphate; NPX, Naproxen Sodium; FLX, Fluoxetine HCl; LRT, Loratadine; OMP, Omeprazole Sodium; RTN, Ritonavir; LPN, Lopinavir; DOX, Doxycycline; RBV, Ribavirin. Error bars show standard deviations ($n = 3$).

achieve sufficient efficacy as monotherapies. It is important to note that for many of the top-ranked combinations, the component therapies exhibited unfavorable efficacy when delivered as monotherapies, but played a key role in mediating optimal efficacy when co-administered. As an example, for Amantadine HCl, Chloroquine Diphosphate, and Omeprazole Sodium, monotherapy was shown to be relatively ineffective at high doses. Compared to no drug treatment, Amantadine (HCl) treatment exhibited infection rates of ≈75%. Chloroquine Diphosphate treatment exhibited infection rates of ≈25%, and Omeprazole Sodium treatment exhibited infection rates of ≈50%. To further evaluate the importance of drug and dose optimization in systematic combination therapy design, it is important to note that Optimal Combo 1 and Sub-Optimal Combo 2 were comprised of the same therapies, but at different doses. This alone resulted in infection rates of 1.5% and 10.7%, an approximately sevenfold difference in efficacy and demonstrating the importance of simultaneous drug and dose optimization. This is further confirmed by the scenario where replacing Amantadine HCl with Omeprazole Sodium and administering this combination at a sub-optimal dose results in a 21.6% infection rate. This represents a 14-fold difference in efficacy compared to Optimal Combo 1. With regards to the factors contributing toward the optimal treatment outcomes, analysis of the interaction terms showed

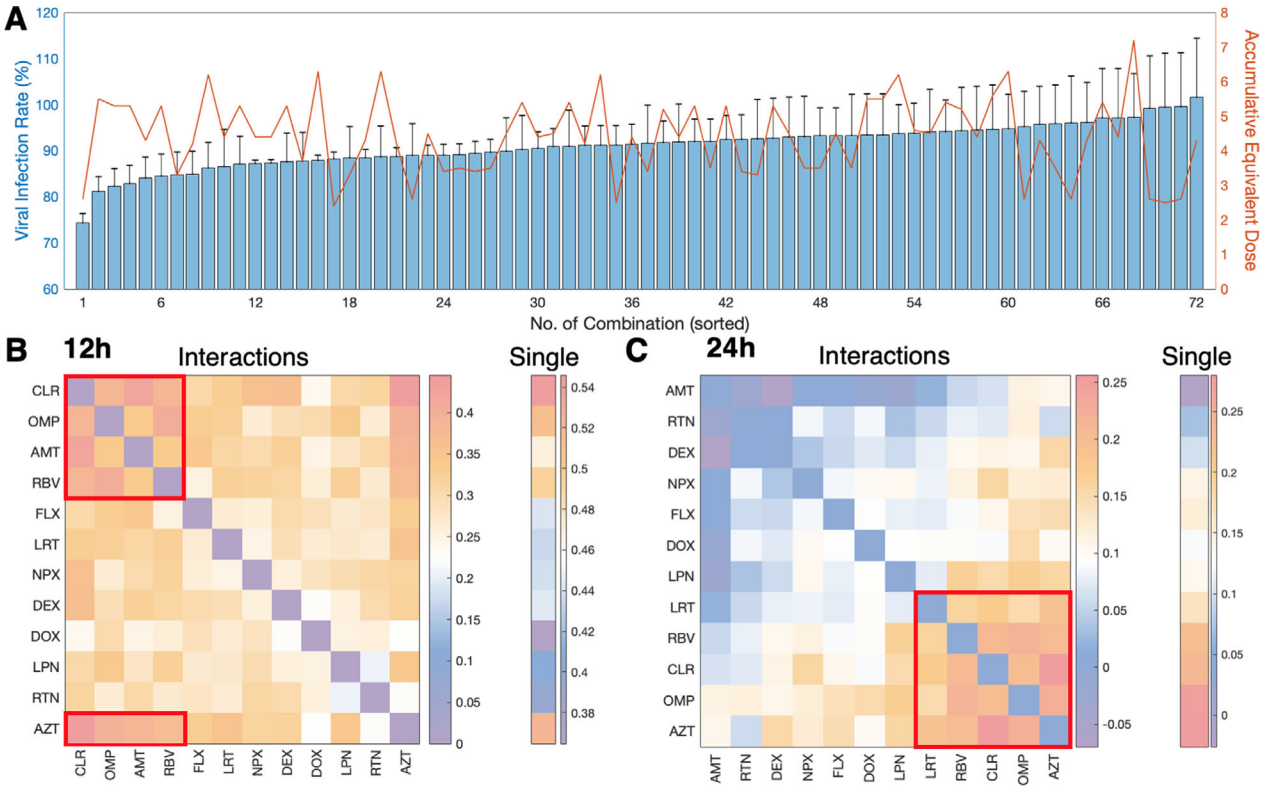

Figure 3. Systematic optimization of 12 drugs in combination with AI-medicine. A) Efficacy of the 72 anti-viral drug combinations. Viral infection rates compared to no drug treatment at 12 h (bar plot and left *y*-axis) of the 72 combinations and their accumulative equivalent doses (line plot and right *y*-axis). Error bars show standard deviations ($n = 3$). The anti-viral scores of each single drug and their quantatitive interactions with other drugs at B) 12 h and C) 24 h are provided. The ranks of drugs were determined by hierarchical clustering. The top 5 contributing drugs and their interactions are tagged with red boxes. Abbreviations: AMT, Amantadine HCl; NPX, Naproxen Sodium; RTN, Ritonavir; DEX, Dexamethasone; FLX, Fluoxetine HCl; LPN, Lopinavir; AZT, Azithromycin; LRT, Loratadine; DOX, Doxycycline; CLR, Chloroquine Diphosphate; OMP, Omeprazole Sodium; RBV, Ribavirin.

that the effects were primarily due to single-drug contributions, drug quadratic effects, 2-drug interaction synergy as well as 3-drug interaction synergy (Figure 4E; Equation S2–S4, Supporting Information).

Fluorescence microscopy was also used to further evaluate the viral infection rate for optimal drug combinations and the nonoptimal drug combinations (**Figure 5**). Of note, no apparent adverse effects cell density for Optimal Combo 1 and 2 were observed. The identification and validation process implemented during Project IDentif.AI demonstrated that rapid optimization of the combination therapy development roadmap could be completed within 3 days (**Figure 6**).

3. Discussion

3.1. The Role of AI toward Optimizing Combinatorial Drug Repurposing

During the COVID-19 outbreak, immediately deployable combination therapies based on drug repurposing were used in the clinic. These included Kaletra (ritonavir/lopinavir) in combination with oseltamivir. (Tamiflu®), and other regimens. Repurposed monotherapies and combination therapies carry the benefit of previously demonstrated safety in patients and threshold efficacy for other indications. Therefore, it is common in these scenarios to select a small pool of established therapies to co-administer, and to adjust drug doses accordingly if toxicity issues ensue. While shown to be potentially clinically effective for some patients, this is largely a trial-and-error strategy. Globally optimizing drug repurposing is a starkly different approach, and can yield combinations comprised of unexpected therapies that far outperform traditional drug combination development, which is based on target/mechanism-based drug selection followed by dose finding.

When not constrained by drug selection based on targets and mechanism of action, the pool of candidate therapies can be enlarged to include a broader diversity of compounds for repurposing. Unfortunately, it should also be noted that drug dosing not only impacts single drug efficacy and safety. In the context of drug combination design, dosing considerations will also impact the drugs that ultimately comprise the best combinations. This effectively creates a parameter space that is too large to interrogate using brute-force testing of all possible combinations.

Project IDentif.AI sought to overcome this barrier that is pervasive across the drug development roadmap for virtually all indications, and demonstrate that the rapid interrogation of a 12-drug parameter space could be completed within a timespan of days. In lieu of drug selection followed by dose finding, we used a previously established quadratic correlation between the 12-drug

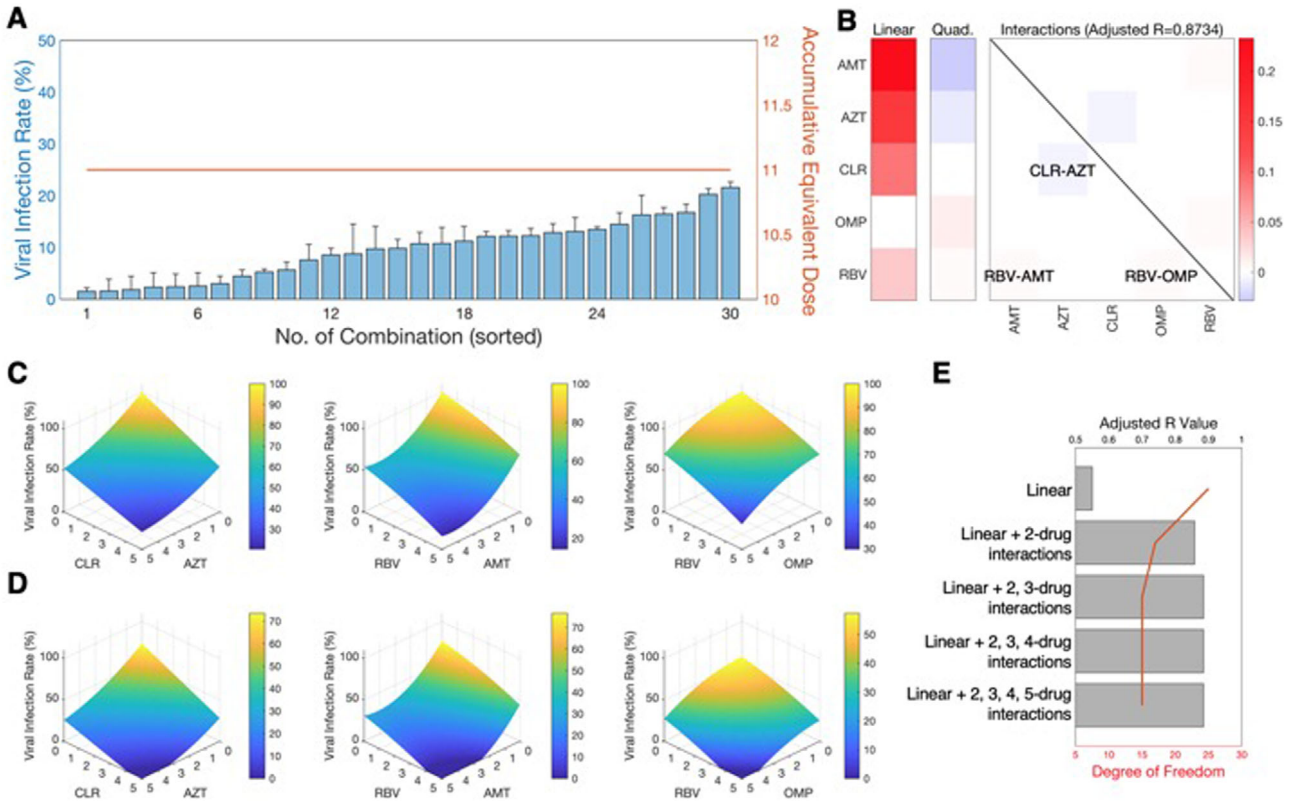

Figure 4. Parabolic response surface analysis of the 5 anti-viral drugs established with the 30 combinations. A) Viral infection rates at 12 h (bar plot and left *y*-axis) of the 30 combinations and their accumulative equivalent doses (line plot and right *y*-axis). Error bars show standard deviations (n = 3). B) The coefficients of the parabolic response surface were calculated by stepwise regression (p-value < 0.001). The values of the coefficients are presented by heatmap. C) Response surfaces of the 3 identified interactions with the other three drugs at 0 dose. The *x*-axis values represent equivalent doses. D) Response surfaces of the 3 identified interactions with the other three drugs at 1 equivalent dose. The *x*-axis values represent equivalent doses. E) The adjusted R values of the polynomial models built by stepwise regression increase as 2-drug and 3-drug interaction terms are added. However, the addition of 4-drug and 5-drug interaction terms makes no difference, indicating the overall anti-viral efficacy is mainly attributed from single drug contributions, drug quadratic effects, 2-drug interaction synergy and 3-drug interaction synergy. Abbreviations: AMT, Amantadine HCl; AZT, Azithromycin; CLR, Chloroquine Diphosphate; OMP, Omeprazole Sodium; RBV, Ribavirin.

Table 1. AI-optimized regimens. Two optimal, sub-optimal, and non-optimal combinations from those experimentally tested during the AI optimization process are shown (units = micromolar).

	Amantadine HCl	Azithromycin	Chloroquine Diphosphate	Omeprazole Sodium	Ribavirin	Viral Infection Rate
Optimal 1	5	5	0.5	0	2.5	1.5%
Optimal 2	5	5	0.5	0.5	0	1.6%
Sub-Optimal 1	0.5	5	0.5	5	0	9.8%
Sub-Optimal 2	0.5	5	5	0	2.5	10.7%
Non-Optimal 1	0	0.5	5	0.5	25	20.3%
Non-Optimal 2	0	0.5	0.5	5	25	21.6%

pool and drug doses (input) as well as inhibition of A549 infection by VSV and A549 viability (outputs) to systematically identify the top drug combinations. This was achieved independent of any prior knowledge of drug targets, mechanism-of-action, or complex disease biology. Furthermore, the implementation of our platform does not require training based on existing data sets or big data. Instead, a specified set of experiments based on a broad spectrum of drug-dose combinations that sufficiently represents the parameter space that is created by the 12-drug set is prospectively conducted. As such, the optimization process is driven completely by prospectively validated data on a cell line or patient sample. Many efforts to evaluate drug sets for single drug treatment or sampled combinations have been conducted. Global optimization of combination therapy design from a large drug set opens up the doors to a broader spectrum of actionable regimens. As our study has shown, even when combinations comprised of

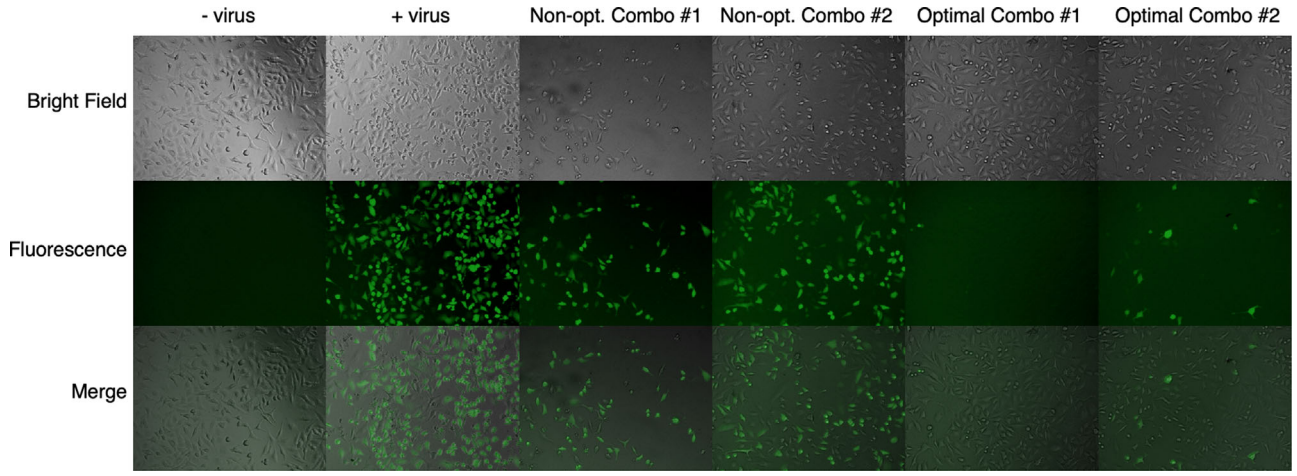

Figure 5. Microscope imaging of optimal and nonoptimal combinations from 5-drug validation test. Optimal drug combinations showed higher viral inhibition rates than nonoptimal combinations. The optimal drug combinations almost completely eradicate viral infection."−virus" indicates the host cells without viral infection, serving as the negative control. "+virus" indicates the host cells with viral infection but without the drug treatment, serving as the positive control. "Non-opt. Combo #1" indicates the host cells with viral infection and concurrent treatment with Nonoptimal Combo 1 (0.5×10^{-6} M Azithromycin, 5×10^{-6} M Chloroquine Diphosphate, 0.5×10^{-6} M Omeprazole Sodium and 25×10^{-6} M Ribavirin). "Non-opt. Combo #2" indicates the host cells with viral infection and concurrent treatment with Nonoptimal Combo 2 (0.5×10^{-6} M Azithromycin, 0.5×10^{-6} M Chloroquine Diphosphate, 5×10^{-6} M Omeprazole Sodium and 25×10^{-6} M Ribavirin). "Optimal Combo #1" indicates the host cells with viral infection and concurrent treatment with Optimal Combo 1 (5×10^{-6} M Amantadine HCl, 5×10^{-6} M Azithromycin, 0.5×10^{-6} M Chloroquine Diphosphate and 25×10^{-6} M Ribavirin). "Optimal Combo #2" indicates the host cells with viral infection and concurrent treatment with Optimal Combo 2 (5×10^{-6} M Amantadine HCl, 5×10^{-6} M Azithromycin, 0.5×10^{-6} M Chloroquine Diphosphate and 0.5×10^{-6} M Omeprazole Sodium) The host cell density = 12k, VSV MOI = 0.1, infection time = 12 h.

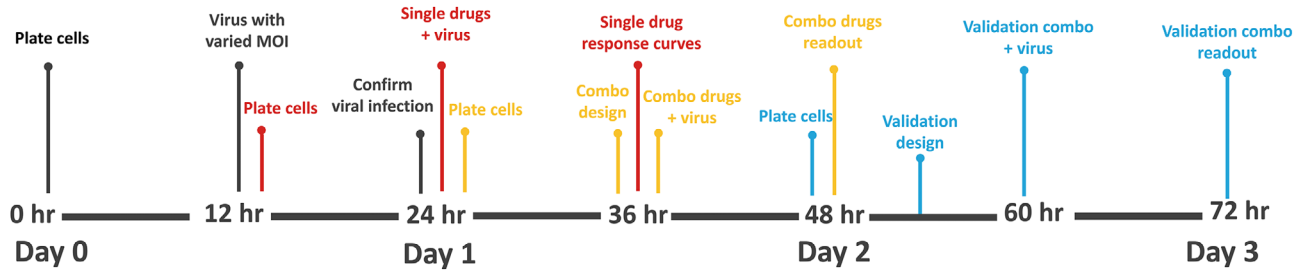

Figure 6. Time line of the optimization platform. The whole optimization process was accomplished within three days after the virus was selected and isolated.

the same drugs are administered at varying doses, a sevenfold difference in efficacy was observed, and even greater differences (14-fold) were observed when one drug was substituted (omeprazole sodium) for another (amantadine HCl, yielding a combination of azithromycin-chloroquine diphosphate-omeprazole sodium-ribavirin) under sub-optimal dosing conditions. This is an interesting finding considering the single drug substitution resulted in such a profound disparity in treatment outcomes, even if all of the drugs considered comprised the top 2 optimal combinations. This further demonstrated the importance of simultaneous drug/dose optimization. Importantly, this process produced multiple drug/dose-optimized combinations within 3 days. This approach has the potential of providing a pipeline of alternatives for patients if issues such as drug resistance are encountered.

It is important to emphasize that this study was conducted using an in vitro VSV model, and the top ranked drug combination has not been subsequently clinically validated. In addition, the VSV model was selected primarily due to it being a well-characterized and readily available platform. If a different disease platform and/or host model are used, it is highly probable that the ranking, drugs that comprise the combinations, and the number of drugs that mediate optimal performance will change. Also, this study was conducted with a diverse range of potential drug candidates. In a clinical setting, especially to address COVID-19 or other clinically relevant pathogens, the pool of drug candidates, which should be developed in consultation with the treating clinical team, is likely to differ substantially from the pool used in this study. Furthermore, if this approach is applied toward clinical samples, patient-specific rankings of optimal combinations can potentially emerge. The importance of the findings of this study are centered on the ability to rapidly interrogate massive parameter spaces that are created when both the right drugs and their right respective doses have to simultaneously reconciled. The ability to reconcile this extraordinarily large set of possible combinations in a timely fashion into actionable and globally optimized combinations may be effective

for scenarios where the prevention of community spread of novel and aggressive pathogens is critical. While additional further clinical validation at the point-of-care is required, several key factors pertaining to the broad clinical relevance and prior validation of technologies related to Project IDentif.AI should be noted. Firstly, previous oncology studies using the quadratic phenotypic optimization platform (QPOP) and CURATE.AI, which are foundational to Project IDentif.AI, have demonstrated that benchtop-based implementation of this approach have directly led to markedly enhanced patient outcomes compared to traditionally observed results.[33,34] Additional clinical validation studies, including one study that harnessed a related AI-guided dosing platform against HIV in humans have further demonstrated the critical importance of drug dosage in mediating optimal treatment efficacy and tolerability.[34,35] Of note, doses that are lower than expected, as well as dosages that were dynamically modulated were commonly used to optimize patient outcomes.

3.2. Harnessing AI toward Global Health: Impact on Healthcare Infrastructure, Policy, Surveillance, and Economics

Deploying AI-optimized infectious disease intervention may result in impact beyond technical and clinical innovation. To scale these platforms toward broader use, healthcare policy, economics, and infrastructure implications as they apply to the patient, payer, and system should be considered. This platform in many ways simultaneously serves as a diagnostic and intervention, because it identifies actionable intervention by calibrating prospectively-obtained patient or population-based data. Added possible benefits include the fact that optimizing drug repurposing to use well-established and potentially cost-effective therapies to manage unpredictable clinical courses, and reductions in treatment complications associated with dose-limiting toxicities and lack of efficacy that may be encountered with trial-and-error/nonoptimized repurposing. These outcomes may lead to reduced healthcare cost burden, which opens up important discussions on how these platforms can be scaled and efficiently integrated into healthcare workflows to enable better informed healthcare spending decisions by patients.[36] These outcomes may also serve as a foundation for broader clinical deployment of AI to intervene effectively at the earlier stages of an epidemic.

Effective tailoring of treatment to both populations and individuals may also increase healthcare quality and efficiency, enabling an opportunity to personalize healthcare costs via quality-based pricing. Specifically, technologies that realize actionable data on patient-specific drug/dose profiles will play a key role in establishing the relationship between individualizing treatment with improved quality of care. This relationship will also be driven by the emergence of quality variation, as some patients, hospital systems, and payers will be more willing than others to make available and/or pay for the testing that may generate more, or better data on patient-specific drug/dose profiles. In turn, this may lead to the introduction of performance-based contracting or quality-based price discrimination, which are suitable pathways to explore, especially if they result in better health outcomes while reducing the cost of care.[37] This concept led to a proposed personalized treatment plan for diabetes patients by using the patients' dose-effect characteristics. They subsequently reported substantial cost reductions and improvements in health outcomes.[37] From the perspective of healthcare providers, financial incentives can improve health care quality, efficiency, and coverage.[38] Many countries have implemented a performance-based approach to contracting for medical services, which has also led to improvements in domains beyond healthcare quality and efficiency. For example, this approach in the U.S. is implemented under the name of "pay for performance" or "payment by results" in the U.K. These strategies have shown that performance-based contracting can improve social welfare,[39] an important consideration considering that pandemic mortality rates have been linked to social inequality, with higher mortality rates being observed with lower socioeconomic status patients.[40] Therefore, in the context of global health and addressing epidemics and pandemics, the impact of AI-guided healthcare will likely expand beyond technical advances and also influence the broader domains of healthcare economics and equality.

In addition to considering patient-centric healthcare coverage of emerging AI platforms to tailor their treatment, as the latest circumstances show on a larger scale, global health emergencies can substantially impact economies. For example, prolonged overburdening of providers, patients, payers and policymakers due to pandemics, coupled with ageing populations can lead to unsustainable healthcare infrastructures. When considering the core disease areas that receive the most attention, such as cancer, diabetes, and cardiovascular, the reality is that communicable infection remains a formidable healthcare infrastructural burden.[41] For example, in many parts of the world, there remains a need to develop better infectious disease interventions to fight the overuse of antibiotics (positioned to consume 10 million lives annually by 2050).[42] This challenge alone could have dramatic economic consequences. Considering the regional relevance of this problem, ≈80% of the malaria parasites in parts of Thailand and Vietnam were resistant to artemisinin and piperaquine, and that the failure rates of the among the most potent frontline combination therapy regimens comprised of dihydroartemisinin-piperaquine (DHA-PPQ) had reached as high as 87% in Northern Thailand.[43] Many solutions ranging from vaccines to novel drug designs are being proposed to address the COVID-19 situation. However, maintaining agility in modulating drug regimens to account for potentially rapid viral mutation or other factors that could dynamically predict patient responses and identify corresponding optimized interventions will be critical. Dengue, which affects more than 400 million people each year, is highly-dynamic based on variables such as geographical climate. A recent study has suggested that 8000 cases of TB could be prevented each year solely through the use of more advanced analytics.[44] The economic evaluation of interventions may become increasingly important as extraordinary circumstances strain healthcare system-wide operations as well as industry operations. Therefore, governments and healthcare systems may be under pressure to substantially impact their quality-adjusted-life-years (QALY) and disability-adjusted-life-years (DALY). It should also be noted that the compound annual growth rate (CAGR) in global spend on drug research and development was 3.6% between 2010 and 2017, outpacing global sales of prescription drugs, which grew at a CAGR of 2.0% during the same period.[45] Further analysis has shown that the

same life expectancy in countries could be achieved at 30% of current healthcare expenditures.[46] Therefore, the importance of accomplishing more while using less resources, making healthcare systems more economically-viable, and maximizing the potential of deploying AI into the agile and dynamic deployment of therapeutic regimens cannot be overstated.

From a global health surveillance perspective, merging and re-emerging infectious diseases will continue to pose a threat to mankind, and it is necessary to develop an arsenal of tools that can be utilized in combatting these pathogens with epidemic/pandemic potential. Based on historical experience, the next big outbreak will be something we have not seen before. In February 2018, The World Health Organization (WHO) added to the R&D Blueprint list of priority of diseases, Disease X.[47] Clade X was previously considered a hypothetical variant of an existing family of organisms that evolved to cause human disease. A preparedness exercise using this modelled pandemic-causing pathogen demonstrated that a lack of actionable interventions could cause devastating global outcomes.[48]

As exhibited with the recent emergence of COVID-19, there are adequate tools to rapidly identify and obtain genomic details in near real time through modern sequencing techniques that often enable the swift development of effective diagnostics.[49] However, the ability to develop medical therapeutics that are both effective and easily deployable remains a critical gap in epidemic response efforts. Vaccines and therapeutics for the past two outbreaks have benefited from greater than 20 years of development efforts that allowed for rapid advancement to human use clinical studies. In epidemic situations interventions that address both individual patient illness and control/prevention of continued transmission are necessary. The spectrum of disease caused by emerging/re-emerging infectious diseases can vary considerably including severe symptomatic disease, moderate/mild symptomatic disease, and asymptomatic spreaders. Moreover, convalescence remains a challenge as recovering patients may continue to shed virus, sometimes for extended periods of time after initial infection. Therefore, effective therapeutics and interventions must have the ability to address the full spectrum of disease and contribute to controlling transmission and spread of the pathogen.

Recently, efforts around monoclonal antibodies (Mabs) have been proposed as a possible solution.[50] While traditional development times for Mabs frame (6 months to years), overall costs (≥$100 per gram),[51] and laborious clinical administration (intravenous), has previously limited their utility in emergency situations, especially in austere and resource-limited clinical settings, substantial efforts have been directed to overcome these challenges.[52] This will play a key role in bringing these critically important and potentially high-efficacy and high-specificity interventions toward broader use. Numerous efforts have considered drug repurposing for infectious disease indications as an approach to quickly respond to an outbreak. Small molecule therapeutics are ideal for rapid deployment in response to an epidemic because they are often stable at room temperature, easily available and have known human pharmacokinetic and safety profiles.[53]

Most successful cases of drug repurposing have been largely serendipitous clinical discoveries, however tremendous effort has also been focused on rational drug repurposing through pathogenic phenotypic in silico and in vitro screening efforts. How these drugs works are often complex and can be on-target or off-target of the original indication. On-target mechanisms of action(s) (MOAs) are often useful targets to block pathogen attachment, entry, and replication within the host. Existing viral drugs are usually the first to be applied to novel viral threats. An additional benefit with repurposed molecules is their potential off-target impacts on a pathogen. These off-target effects are usually harder to define during development.

A major challenge in drug repurposing efforts is that few drugs demonstrate the safety and potency alone to achieve therapeutic antiviral activity. Therefore, studies have focused on combinational strategies to meet the potency and safety dose requirements to be considered in response to a new threat.[54] These efforts rely on in vitro and in vivo testing to evaluate and can be considerably difficult to demonstrate, even with two drug combinations.[55] In vitro and especially in vivo testing of single drugs or combinations can be a lengthy process (months to years).[56] Higher complexity combinational approaches offer the greatest benefit, but traditional methods developing higher-order combinations . Emerging in silico modelling and AI approaches that are driven by prospective experimental validation are converging to allow for potentially rapid responses to outbreak and pandemic events.[7,32,57] The approach described here, and other recently reported methods are key steps to higher order combinational treatment formulations that overcomes past limitations with repurposing and will allow for disease specific and likely personalized antivirals.[58] The optimized combinations in Table 1 were derived and identified from those experimentally tested, and thus further studies using the optimized combinations as determined from IDentif.AI will be required.

4. Conclusion

This work has provided a foundation toward the rapid identification of dynamically optimized and actionable combination therapies to address a broad spectrum of infectious disease applications while also accounting for new strains that may eventually circulate. Given the mechanism- and disease-agnostic foundation of Project IDentif.AI, further studies will evaluate this platform for rapid COVID-19 intervention, and establish its readiness to pinpoint regimens toward downstream pathogens with aggressive clinical courses. Pairing the technical capabilities of AI-driven drug development platforms with important policy-based considerations and lessons learned from the global response to SARS, H1N1, EVD, and other epidemics/pandemics may ultimately lead to expedited intervention at scale.

5. Experimental Section

Cell Culture: The lung cancer cell line (A549, ATCC, USA) was cultured in high-glucose Dulbecco's modified Eagle's medium (DMEM) (Invitrogen, USA) that was supplemented with 10% fetal bovine serum (FBS) (Invitrogen, USA) and 1% penicillin–streptomycin (Invitrogen, USA). The culture was maintained at 37 °C containing 5% v/v CO_2 and the cells were harvested upon reaching 80% confluence. 100 µL of cell suspension (4–12k cells per well) was seeded in 96-well plates and pre-incubated for 12 h for treatment with the candidate drugs and viral platform. Cells without any drug treatment and without viral infection served as a control. Each condition was run in triplicate. Drug-induced cytotoxicity was

measured using a cell counting kit-8 (CCK8, DOJINDO, Japan). Briefly, 15 µL of CCK8 solution was added to each well containing 150 µL solution and then incubated for 2 h at 37 °C in order to conduct the cytotoxicity assay. The cell viability was assessed by measuring the absorbance (450 nm) via a microplate reader (BioTek, Synergy HT, USA).

Viral Infection and Plate Reader: Vesicular stomatitis virus (VSV), a RNA virus, was used as the pathogen model in this work. VSV was engineered and encoded with green fluorescent protein (GFP). The concentration of VSV stock was 1×10^4 pfu μL^{-1}, and different multiplicity of infection (MOI) parameters were used to optimize the final MOI for cell infection. The MOI used for the optimization process included 1, 0.5, 0.25, 0.125, 0.1, 0.01, and 0.001 and 0 (control). Cells were infected by VSV under different MOI parameters for 12, 24, and 30 h during the optimization process. For each MOI, the conditions were run in triplicate. 100 µL of cell suspension (12k cells per well) was seeded in a 96 well-plate and pre-incubated for 12 h to be infected by VSV. Following viral infection, the GFP fluorescence intensity of the cells induced by VSV reproduction was measured with a microplate reader (BioTek, Synergy HT, USA) using the top-reading mode, with excitation wavelength of 483 nm, and emission wavelength of 535 nm).

Dilution of Candidate Therapies: 12 drugs purchased from Selleckchem (TX, USA) were included in this study. These included amantadine HCl, dexamethasone, azithromycin, chloroquine diphosphate, naproxen sodium, fluoxetine HCl, loratadine, omeprazole sodium, ritonavir, lopinavir, doxycycline and ribavirin. Amantadine HCl, chloroquine diphosphate, naproxen sodium, fluoxetine HCl, omeprazole sodium, doxycycline and ribavirin were diluted using complete cell culture medium, while dexamethasone, azithromycin, loratadine, ritonavir, and lopinavir were diluted in DMSO. The final stock concentration of all the drugs was 100×10^{-3} M. With the exception of naproxen sodium and ribavirin, the other 10 drugs were further diluted for four concentrations including 0.1, 1, 10, and 100×10^{-6} M during the drug optimization process. The concentrations of naproxen sodium and ribavirin during the drug optimization process were 0.5, 5, 50, and 500×10^{-6} M. The maximum possible final concentration of DMSO added to the cells for monotherapies and combination therapies was 0.3% for both. During the drug optimization process, triplicates were run per treatment condition.

Design-Of-Experiment (DOE): The experimental design of the first stage of testing was generated according to uniform design theory.[59] 72 combinations were chosen with the largest sum of multi-drug interaction distances and smallest variance of accumulative doses from trillions of randomly generated experiment designs. The design of the second stage of validation was generated according to orthogonal array design (OAD).

Accumulative Equivalent Dose: To cancel the disparity of the therapeutic concentration ranges between drugs, as well as to facilitate the expression of dose concentrations, the concept of equivalent dose was adopted. 1 equivalent dose refers to 5×10^{-6} M for naproxen sodium and ribavirin, and 1×10^{-6} M for the others. Thus, the accumulative equivalent dose of a combination therapy was defined as the sum of the equivalent doses of its constituents.

Data Analysis: The parabolic response surface analysis and multi-drug interaction regression analysis were conducted via the build-in function "stepwiselm" in MATLAB 2018a with self-written code. The algorithm derived a quadratic model accounting for collinearity using the bidirectional elimination approach with the adjusted *R*-value as selection criterion.

The STRICT algorithm was used to identify quantitative drug interactions. STRICT is a scoring algorithm based on projection distance, which assesses the capacity of infection inhibition by giving an anti-viral score to each drug and pairwise interaction in this study.[60] Consider a combination $k = (x_{k,1}, x_{k,2}, \ldots, x_{k,n})$, the normalized Euclidean distance from point k to the projection p on axis i is

$$D_{k,i} = \sqrt{\frac{\sum_{s \neq i} x_{k,s}^2}{n-1}}$$

Where $D_{k,i}$ is normalized to [0,1], and mapped with a decreasing function:

$$f\left(D_{k,i}\right) = \left(1 - D_{k,i}\right)^q$$

The single drug STRICT score is then defined as the sum of the productions of the outputs, projections, and the function of the distance, which can be denoted as

$$Score_i = \sum_{k=1}^{m} Y_k \cdot x_{k,i} \cdot f\left(D_{k,i}\right)$$

Using this definition, the STRICT score can be easily expanded to multi-drug interactions, if point k is projected to plane i, j instead of axis i. The normalized distance is

$$D_{k,i} = \sqrt{\frac{\sum_{s \neq i,j} x_{k,s}^2}{n-2}}$$

Thus, the drug-pair STRICT score can be defined as

$$Score_{i,j} = \sum_{k=1}^{m} Y_k \cdot \sqrt{x_{k,i} \cdot x_{k,j}} \cdot f\left(D_{k,i,j}\right)$$

Supporting Information

Supporting Information is available from the Wiley Online Library or from the author.

Acknowledgements

A.A. and B.W. contributed equally to this work. X.D. gratefully acknowledges support from Shanghai Municipal Science and Technology (2017SHZDZX01), National Key Research and Development Program of China (2017ZX10203205-006-002) and National Natural Science Foundation of China (81871448). D.H. gratefully acknowledges the Office of the President, Office of the Senior Deputy President and Provost, and Office of the Deputy President of Research and Technology at the National University of Singapore for supporting this study. The authors also gratefully acknowledge Poonam Rai for her substantial efforts toward expediting the initiation of this project, as well as Peter Wang for manuscript review. D.H. acknowledges support from a Ministry of Education (MOE) Tier 1 FRC grant and Singapore Ministry of Health's National Medical Research Council under its Open Fund-Large Collaborative Grant ("OF-LCG") (MOH-OFLCG18May-0003).

Conflict of Interest

T.K., A.B., E.K.C., D.H., and X.D. are inventors of pending and issued patents pertaining to artificial intelligence-based drug development and personalized medicine.

Keywords

artificial intelligence, combination therapy, COVID-19, digital medicine, infectious diseases

Received: February 23, 2020
Published online: April 16, 2020

[1] a) N. Zhu, D. Zhang, W. Wang, X. Li, B. Yang, J. Song, X. Zhao, B. Huang, W. Shi, R. Lu, P. Niu, F. Zhan, X. Ma, D. Wang, W. Xu, G.

Wu, G. F. Gao, W. Tan, China Novel Coronavirus Investigating and Research Team, *N. Engl. J. Med.* **2020**, *382*, 727; b) M. L. Holshue, C. DeBolt, S. Lindquist, K. H. Lofy, J. Wiesman, H. Bruce, C. Spitters, K. Ericson, S. Wilkerson, A. Tural, G. Diaz, A. Cohn, L. Fox, A. Patel, S. I. Gerber, L. Kim, S. Tong, X. Lu, S. Lindstrom, M. A. Pallansch, W. C. Weldon, H. M. Biggs, T. M. Uyeki, S. K. Pillai, Washington State 2019-nCoV Case Investigation Team, *N. Engl. J. Med.* **2020**, *382*, 929; c) C. Rothe, M. Schunk, P. Sothmann, G. Bretzel, G. Froeschl, C. Wallrauch, T. Zimmer, V. Thiel, C. Janke, W. Guggemos, M. Seilmaier, C. Drosten, P. Vollmar, K. Zwirglmaier, S. Zange, R. Wolfel, M. Hoelscher, *N. Engl. J. Med.* **2020**, *382*, 970; d) Q. Li, X. Guan, P. Wu, X. Wang, L. Zhou, Y. Tong, R. Ren, K. S. M. Leung, E. H. Y. Lau, J. Y. Wong, X. Xing, N. Xiang, Y. Wu, C. Li, Q. Chen, D. Li, T. Liu, J. Zhao, M. Liu, W. Tu, C. Chen, L. Jin, R. Yang, Q. Wang, S. Zhou, R. Wang, H. Liu, Y. Luo, Y. Liu, G. Shao, H. Li, Z. Tao, Y. Yang, Z. Deng, B. Liu, Z. Ma, Y. Zhang, G. Shi, T. T. Y. Lam, J. T. Wu, G. F. Gao, B. J. Cowling, B. Yang, G. M. Leung, Z. Feng, *N. Engl. J. Med.* **2020**, *382*, 1199; e) V. J. Munster, M. Koopmans, N. van Doremalen, D. van Riel, E. de Wit, *N. Engl. J. Med.* **2020**, *382*, 692.

[2] J. S. Peiris, K. Y. Yuen, A. D. Osterhaus, K. Stöhr, *N. Engl. J. Med.* **2003**, *349*, 2431.

[3] E. Bautista, T. Chotpitayasunondh, Z. Gao, S. A. Harper, M. Shaw, T. M. Uyeki, S. R. Zaki, F. G. Hayden, D. S. Hui, J. D. Kettner, A. Kumar, M. Lim, N. Shindo, C. Penn, K. G. Nicholson, *N. Engl. J. Med.* **2010**, *362*, 1708.

[4] R. Gao, B. Cao, Y. Hu, Z. Feng, D. Wang, W. Hu, J. Chen, Z. Jie, H. Qiu, K. Xu, X. Xu, H. Lu, W. Zhu, Z. Gao, N. Xiang, Y. Shen, Z. He, Y. Gu, Z. Zhang, Y. Yang, X. Zhao, L. Zhou, X. Li, S. Zou, Y. Zhang, X. Li, L. Yang, J. Guo, J. Dong, Q. Li, L. Dong, Y. Zhu, T. Bai, S. Wang, P. Hao, W. Yang, Y. Zhang, J. Han, H. Yu, D. Li, G. F. Gao, G. Wu, Y. Wang, Z. Yuan, Y. Shu, *N. Engl. J. Med.* **2013**, *368*, 1888.

[5] Y. M. Arabi, H. H. Balkhy, F. G. Hayden, A. Bouchama, T. Luke, J. K. Baillie, A. Al-Omari, A. H. Hajeer, M. Senga, M. R. Denison, J. S. Nguyen-Van-Tam, N. Shindo, A. Bermingham, J. D. Chappell, M. D. Van Kerkhove, R. A. Fowler, *N. Engl. J. Med.* **2017**, *376*, 584.

[6] S. Mulangu, L. E. Dodd, R. T. Davey Jr, O. Tshiani Mbaya, M. Proschan, D. Mukadi, M. Lusakibanza Manzo, D. Nzolo, A. Tshomba Oloma, A. Ibanda, R. Ali, S. Coulibaly, A. C. Levine, R. Grais, J. Diaz, H. C. Lane, J. J. Muyembe-Tamfum, *N. Engl. J. Med.* **2019**, *381*, 2293.

[7] a) A. Zimmer, I. Katzir, E. Dekel, A. E. Mayo, U. Alon, *Proc. Natl. Acad. Sci. USA* **2016**, *113*, 10442; b) I. Katzir, M. Cokol, B. B. Aldridge, U. Alon, *PLoS Comput. Biol.* **2019**, *15*, 1006774; c) E. Tekin, C. Beppler, C. White, Z. Mao, V. M. Savage, P. J. Yeh, *J. R. Soc., Interface* **2016**, *13*, 20160332; d) Z. B. Weinstein, N. Kuru, S. Kiriakov, A. C. Palmer, A. S. Khalil, P. A. Clemons, M. H. Zaman, F. P. Roth, M. Cokol, *Nat. Commun.* **2018**, *9*, 1; e) C. R. MacNair, J. M. Stokes, L. A. Carfrae, A. A. Fiebig-Comyn, B. K. Coombes, M. R. Mulvey, E. D. Brown, *Nat. Commun.* **2018**, *9*, 1; f) P. D. Tamma, S. E. Cosgrove, L. L. Maragakis, *Clin. Microbiol. Rev.* **2012**, *25*, 450; g) M. Baym, L. K. Stone, R. Kishony, *Science* **2016**, *351*, aad3292; h) T. Brennan-Krohn, J. E. Kirby, *Antimicrob. Agents Chemother.* **2019**, *AAC*, 01374.

[8] A. Maxmen, *Nature* **2020**, *578*, 347.

[9] T. Nisar, H. Sutherland-Foggio, W. Husar, *Lancet Neurol.* **2019**, *18*, 1080.

[10] R. S. Schwab, A. C. England, Jr., D. C. Poskanzer, R. R. Young, *JAMA, J. Am. Med. Assoc.* **1969**, *208*, 1168.

[11] R. A. Cohen, M. Fisher, *Arch. Neurol.* **1989**, *46*, 676.

[12] J. de Gans, D. van de Beek, *N. Engl. J. Med.* **2002**, *347*, 1549.

[13] W. F. Wan Jamaludin, P. Periyasamy, W. R. Wan Mat, S. F. Abdul Wahid, *J. Clin. Virol.* **2015**, *69*, 91.

[14] M. Laopaiboon, R. Panpanich, K. Swa Mya, *Cochrane Database Syst. Rev.* **2015**, https://doi.org/10.1002/14651858.CD001954.pub4

[15] M. Izadi, B. Dadsetan, Z. Najafi, S. Jafari, E. Mazaheri, O. Dadras, H. Heidari, S. SeyedAlinaghi, F. Voltarelli, *Recent Pat. Anti-Infect. Drug Discovery* **2018**, *13*, 228.

[16] M. W. Dunne, N. Singh, M. Shukla, N. Valecha, P. C. Bhattacharyya, V. Dev, K. Patel, M. K. Mohapatra, J. Lakhani, R. Benner, C. Lele, K. Patki, *J. Infect. Dis.* **2005**, *191*, 1582.

[17] D. Plantone, T. Koudriavtseva, *Clin Microbiol. Infect.* **2018**, *38*, 653.

[18] P. A. Todd, S. P. Clissold, *Drugs* **1990**, *40*, 91.

[19] W. Zheng, W. Fan, S. Zhang, P. Jiao, Y. Shang, L. Cui, M. Mahesutihan, J. Li, D. Wang, G. F. Gao, L. Sun, W. Liu, *Cell Rep.* **2019**, *27*, 1875.

[20] D. T. Wong, K. W. Perry, F. P. Bymaster, *Nat. Rev. Drug Discovery* **2005**, *4*, 764.

[21] J. Zuo, K. K. Quinn, S. Kye, P. Cooper, R. Damoiseaux, P. Krogstad, *Antimicrob. Agents Chemother.* **2012**, *56*, 4838.

[22] a) T. M. Nolen, *Clin. Ther.* **1997**, *19*, 39; b) S. P. Clissold, E. M. Sorkin, K. L. Goa, *Drugs* **1989**, *37*, 42.

[23] a) J. J. Kirshner, M. C. McDonald, F. Kruter, A. S. Guinigundo, L. Vanni, C. L. Maxwell, M. Reiner, T. E. Upchurch, J. Garcia, P. K. Morrow, *Supportive Care Cancer* **2018**, *26*, 1323; b) K. Moore, R. Haroz, *J. Emerg. Med.* **2017**, *52*, e29.

[24] a) P. N. Maton, *N. Engl. J. Med.* **1991**, *324*, 965; b) L. Olbe, E. Carlsson, P. Lindberg, *Nat. Rev. Drug Discovery* **2003**, *2*, 132.

[25] a) A. Udelnow, A. Kreyes, S. Ellinger, K. Landfester, P. Walther, T. Klapperstueck, J. Wohlrab, D. Henne-Bruns, U. Knippschild, P. Würl, *PLoS One* **2011**, *6*, e20143; b) U.-H. Jin, S.-O. Lee, C. Pfent, S. Safe, *BMC Cancer* **2014**, *14*, 498; c) L.-Y. Yu, L.-N. Sun, X.-H. Zhang, Y.-Q. Li, L. Yu, L. Meng, H.-W. Zhang, Y.-Q. Wang, *Adv. Ther.* **2017**, *34*, 1070.

[26] R. S. Cvetkovic, K. L. Goa, *Drugs* **2003**, *63*, 2769.

[27] C. Chu, V. Cheng, I. Hung, M. Wong, K. Chan, K. Chan, R. Kao, L. Poon, C. Wong, Y. Guan, J. Peiris, K. Yuen, *Thorax* **2004**, *59*, 252.

[28] N. Joshi, D. Q. Miller, *Arch. Intern. Med.* **1997**, *157*, 1421.

[29] a) T. Van Zele, P. Gevaert, G. Holtappels, A. Beule, P. J. Wormald, S. Mayr, G. Hens, P. Hellings, F. A. Ebbens, W. Fokkens, P. Van Cauwenberge, C. Bauchert, *J. Allergy Clin. Immunol.* **2010**, *125*, 10669; b) J. Q. Del Rosso, G. F. Webster, M. Jackson, M. Rendon, P. Rich, H. Torok, M. Bradshaw, *J. Am. Acad. Dermatol.* **2007**, *56*, 791.

[30] M. W. Fried, M. L. Shiffman, K. R. Reddy, C. Smith, G. Marinos, F. L. Gonçales Jr, D. Häussinger, M. Diago, G. Carosi, D. Dhumeaux, A. Craxi, A. Lin, J. Hoffman, J. Yu, *N. Engl. J. Med.* **2002**, *347*, 975.

[31] a) M. Mardani, M. K. Jahromi, K. H. Naieni, M. Zeinali, *Clin. Infect. Dis.* **2003**, *36*, 1613; b) K. Ventre, A. Randolph, *Cochrane Database Syst. Rev.* **2007**, https://doi.org/10.1002/14651858.CD000181.pub3

[32] a) M. B. M. A. Rashid, T. B. Toh, L. Hooi, A. Silva, Y. Zhang, P. F. Tan, A. L. Teh, N. Karnani, S. Jha, C.-M. Ho, *Sci. Transl. Med.* **2018**, *10*, eaan0941; b) H. Wang, D.-K. Lee, K.-Y. Chen, J.-Y. Chen, K. Zhang, A. Silva, C.-M. Ho, D. Ho, *ACS Nano* **2015**, *9*, 3332; c) M. B. Mohd Abdul Rashid, T. B. Toh, A. Silva, L. Nurrul Abdullah, C.-M. Ho, D. Ho, E. K.-H. Chow, *J. Lab. Autom.* **2015**, *20*, 423; d) D. Ho, A. Zarrinpar, E. K.-H. Chow, *ACS Nano* **2016**; e) D. Ho, C.-H. K. Wang, E. K.-H. Chow, *Sci. Adv.* **2015**, *1*, 1500439; f) J. J. Lim, J. Goh, M. B. M. A. Rashid, E. K. H. Chow, *Adv. Thera.* **2019**, https://doi.org/10.1002/adtp.201900122; g) P. K. Wong, F. Yu, A. Shahangian, G. Cheng, R. Sun, C.-M. Ho, *Proc. Natl. Acad. Sci. USA* **2008**, *105*, 5105; h) I. Al-Shyoukh, F. Yu, J. Feng, K. Yan, S. Dubinett, C.-M. Ho, J. S. Shamma, R. Sun, *BMC Syst. Biol.* **2011**, *5*, 88; i) X. Ding, Z. Njus, T. Kong, W. Su, C.-M. Ho, S. Pandey, *Sci. Adv.* **2017**, *3*, eaao1254; j) P. Nowak-Sliwinska, A. Weiss, X. Ding, P. J. Dyson, H. Van Den Bergh, A. W. Griffioen, C.-M. Ho, *Nat. Protoc.* **2016**, *11*, 302; k) Q. Liu, C. Zhang, X. Ding, H. Deng, D. Zhang, W. Cui, H. Xu, Y. Wang, W. Xu, L. Lv, H. Zhang, Y. He, Q. Wu, M. Szyf, C.-M. Ho, J. Zhu, *Sci. Rep.* **2015**, *5*, 11464; l) A. Weiss, X. Ding, J. R. Van Beijnum, I. Wong, T. J. Wong, R. H. Berndsen, O. Dormond, M. Dallinga, L. Shen, R. O. Schlingemann, R. Pili, C.-M. Ho, P. J. Dyson, H. van den Bergh, A. W. Griffioen, P. Nowak-Sliwinska, *Angiogenesis* **2015**, *18*, 233; m) X. Ding, D. J. Sanchez, A. Shahangian,

I. Al-Shyoukh, G. Cheng, C.-M. Ho, *Int. J. Nanomed.* **2012**, *7*, 2281; n) B.-Y. Lee, D. L. Clemens, A. Silva, B. J. Dillon, S. Masleša-Galić, S. Nava, X. Ding, C.-M. Ho, M. A. Horwitz, *Nat. Commun.* **2017**, *8*, 1; o) A. Silva, B.-Y. Lee, D. L. Clemens, T. Kee, X. Ding, C.-M. Ho, M. A. Horwitz, *Proc. Natl. Acad. Sci. USA* **2016**, *113*, E2172.

[33] S. de Mel, M. B. Rashid, X. Y. Zhang, J. Goh, C. T. Lee, L. M. Poon, E. H. Chan, X. Liu, W. J. Chng, Y. L. Chee, *Blood Cancer J.* **2020**, *10*, 1.

[34] A. J. Pantuck, D. K. Lee, T. Kee, P. Wang, S. Lakhotia, M. H. Silverman, C. Mathis, A. Drakaki, A. S. Belldegrun, C. M. Ho, D. Ho, *Adv. Ther.* **2018**, *1*, 1800104.

[35] a) D. Ho, S. R. Quake, E. R. McCabe, W. J. Chng, E. K. Chow, X. Ding, 54 B. D. Gelb, G. S. Ginsburg, J. Hassenstab, C.-M. Ho, W. C. Mobley, G. P. Nolan, S. T. Rosen, P. Tan, Y. Yen, A. Zarrinpar, *Trends Biotechnol.* **2020**, https://doi.org/10.1016/j.tibtech.2019.12.021; b) A. Zarrinpar, D.-K. Lee, A. Silva, N. Datta, T. Kee, C. Eriksen, K. Weigle, V. Agopian, F. Kaldas, D. Farmer, S. E. Wang, R. Busuttil, C.-M. Ho, D. Ho, *Sci. Transl. Med.* **2016**, *8*, 333ra49; c) T. Kee, C. Weiyan, A. Blasiak, P. Wang, J. K. Chong, J. Chen, B. T. Yeo, D. Ho, C. L. Asplund, *Adv. Ther.* **2019**, *2*, 1900023; d) Y. Shen, T. Liu, J. Chen, X. Li, L. Liu, J. Shen, J. Wang, R. Zhang, M. Sun, Z. Wang, *Adv. Therap.* **2019**, https://doi.org/10.1002/adtp.201900114; e) X. Ding, V. H. Chang, Y. Li, X. Li, H. Xu, C. M. Ho, D. Ho, Y. Yen, *Adv. Therap.* **2019**, https://doi.org/10.1002/adtp.201900127.

[36] a) S. P. Keehan, A. M. Sisko, C. J. Truffer, J. A. Poisal, G. A. Cuckler, A. J. Madison, J. M. Lizonitz, S. D. Smith, *Health Affairs* **2011**, *30*, 1594; b) U. E. Reinhardt, *Health Affairs* **2006**, *25*, 57; c) U. E. Reinhardt, *Health Affairs* **2011**, *30*, 2125.

[37] E. K. Lee, X. Wei, F. Baker-Witt, M. D. Wright, A. Quarshie, *Interfaces* **2018**, *48*, 422.

[38] a) M. Batty, B. Ippolito, *Am. Econ. J.: Econ. Policy* **2017**, *9*, 28; b) P. Dubois, L. Lasio, *Am. Econ. Rev.* **2018**, *108*, 3685.

[39] E. Adida, F. Bravo, *Manage. Sci.* **2019**, *65*, 1322.

[40] S.-E. Mamelund, *Tidsskr. Nor. Laegeforen.* **2017**, *137*, 911.

[41] I. Gupta, P. Guin, *Bull W. H O.* **2010**, *88*, 199.

[42] M. E. de Kraker, A. J. Stewardson, S. Harbarth, *PLoS Med.* **2016**, *13*, e1002184.

[43] a) R. Amato, R. D. Pearson, J. Almagro-Garcia, C. Amaratunga, P. Lim, S. Suon, S. Sreng, E. Drury, J. Stalker, O. Miotto, R. M. Fairhurst, D. P. Kwiatkowski, *Lancet Infect. Dis.* **2018**, *18*, 337; b) V. Thamlikitkul, V. Tangcharoensathien, N. Bhamarapravati, *AIDS in Asia*, Vol. *269*, Springer, New York **2004**; c) M. Imwong, K. Suwannasin, C. Kunasol, K. Sutawong, M. Mayxay, H. Rekol, F. M. Smithuis, T. M. Hlaing, K. M. Tun, R. W. van der Pluijm, R. Tripura, O. Miotto, D. Menard, M. Dhorda, N. P. J. Day, N. J. White, *Lancet Infect. Dis.* **2017**, *17*, 491.

[44] a) B. Wilder, S.-C. Suen, M. Tambe, *Thirty-Second AAAI Conf. on Artificial Intelligence*, AAAI, Palo Alto, California **2018**; b) C. I. Siettos, L. Russo, *Virulence* **2013**, *4*, 295.

[45] S. Sancheti, H. Thomas, R. van den Heuvel, A. Verhaeghe, C. Rivett, *R&D 2030. Reinvent innovation and become an R&D front-runner by 2030*, KPMG International, Switzerland **2018**.

[46] D. E. Bloom, D. M. Cadarette, J. Roland, J. Sullivan, *Misaligned Stakeholders and Health System Underperformance*, Working Paper no. 134, Program on the Global Demography of Aging (PGDA), Boston, Massachusetts **2017**.

[47] W. H. O. https://www.who.int/activities/prioritizing-diseases-for-research-and-development-in-emergency-contexts (accessed: February 2020).

[48] C. Watson, E. S. Toner, M. P. Shearer, C. Rivers, D. Meyer, C. Hurtado, M. Watson, G. K. Gronvall, A. A. Adalja, T. K. Sell, T. Inglesby, A. Cicero, *Health Security* **2019**, *17*, 410.

[49] L. F. Ng, I. Barr, T. Nguyen, S. M. Noor, R. S.-P. Tan, L. V. Agathe, S. Gupta, H. Khalil, T. L. To, S. S. Hassan, E.-C. Ren, *BMC Infect. Dis.* **2006**, *6*, 40.

[50] a) G. G. Olinger, J. Pettitt, D. Kim, C. Working, O. Bohorov, B. Bratcher, E. Hiatt, S. D. Hume, A. K. Johnson, J. Morton, M. Pauly, K. J. Whaley, C. M. Lear, J. E. Biggins, C. Scully, L. Hensley, L. Zeitlin, *Proc. Natl. Acad. Sci.* **2012**, *109*, 18030; b) J. Pettitt, L. Zeitlin, D. H. Kim, C. Working, J. C. Johnson, O. Bohorov, B. Bratcher, E. Hiatt, S. D. Hume, A. K. Johnson, J. Morton, M. H. Pauly, K. J. Whaley, M. F. Ingram, A. Zovanyi, M. Heinrich, A. Piper, J. Zelko, G. G. Olinger, *Sci. Transl. Med.* **2013**, *5*, 199ra113; c) E. P. Teoh, P. Kukkaro, E. W. Teo, A. P. Lim, T. T. Tan, A. Yip, W. Schul, M. Aung, V. A. Kostyuchenko, Y. S. Leo, S. H. Chan, K. G. C. Smith, A. H. Y. Chan, G. Zou, E. E. Ooi, D. M. Kemeny, J. K. W. Ng, S. Alonso, D. Fisher, P.-Y. Shi, B. J. Hanson, S.-M. Lok, P. A. MacAry, *Sci. Transl. Med.* **2012**, *4*, 139ra83.

[51] E. Sparrow, M. Friede, M. Sheikh, S. Torvaldsen, *Bull W. H O.* **2017**, *95*, 235.

[52] N. Fleming, *Nature* **2018**, *557*, S55.

[53] J. Dyall, J. C. Johnson, E. Postnikova, Y. Cong, H. Zhou, D. M. Gerhardt, J. Michelotti, A. N. Honko, S. Kern, L. E. DeWald, K. G. O'Loughlin, C. E. Green, J. C. Mirsalis, R. S. Bennett, G. G. Olinger, P. B. Jahrling, L. E. Hensley, *J. Infect. Dis.* **2018**, *218*, S592.

[54] M. Wang, R. Cao, L. Zhang, X. Yang, J. Liu, M. Xu, Z. Shi, Z. Hu, W. Zhong, G. Xiao, *Cell Res.* **2020**, *30*, 269.

[55] Y.-S. Cheng, P. R. Williamson, W. Zheng, *Curr. Opin. Pharmacol.* **2019**, *48*, 92.

[56] A. Talevi, C. L. Bellera, *Expert Opin. Drug Discov.* **2019**, *15*, 397.

[57] a) S. L. Prashad, L. Drusbosky, H. Sibai, M. D. Minden, S. J. Western, C. Biondi, R. Shah, D. Liu, T. Nguyen, C. Warnock, P. Quinzio, D. S. Matthew, Matthew, E. Traer, C. R. Cogle, A. D. Schimmer, D. Heiser, *Fifty-Eight ASH Annual Meeting*, ASH, Washington, DC **2016**, https://doi.org/10.1182/blood.V128.22.5206.5206; b) A. Aleshin, B. C. Medeiros, S. Kamble, D. Heiser, M. Santaguida, S. Prashad, P. L. Greenberg, *AACR Annual Meeting 2018*, AACR, Philadelphia, Philadelphia **2018**, https://doi.org/10.1158/1538-7445.AM2018-568; c) Y.-C. Chen, F. Farzadfard, N. Gharaei, W. C. Chen, J. Cao, T. K. Lu, *Mol. Cell* **2017**, *68*, 247; d) I. Wallach, M. Dzamba, A. Heifets, *arXiv preprint* arXiv:1510.02855 **2015**; e) A. Zhavoronkov, Y. A. Ivanenkov, A. Aliper, M. S. Veselov, V. A. Aladinskiy, A. V. Aladinskaya, V. A. Terentiev, D. A. Polykovskiy, M. D. Kuznetsov, A. Asadulaev, Y. Volkov, A. Zholus, R. R. Shayakhmetov, A. Zhebrak, L. I. Minaeva, B. A. Zagribelnyy, L. H. Lee, R. Soll, D. Madge, L. Xing, T. Guo, A. Aspuru-Guzik, *Nat. Biotechnol.* **2019**, *27 37*, 1038.

[58] a) F. Sohraby, M. Bagheri, H. Aryapour, in *Computational Methods for Drug Repurposing*, Springer, New York **2019**, 23; b) M. Kontoyianni, in *Proteomics for Drug Discovery*, Springer, New York **2017**, 255.

[59] K.-T. Fang, D. K. Lin, P. Winker, Y. Zhang, *Technometrics* **2000**, *42*, 237.

[60] J. Sun, B. Wang, A. R. Warden, D. Cui, X. Ding, *Anal. Chem.* **2019**, *91*, 13562.